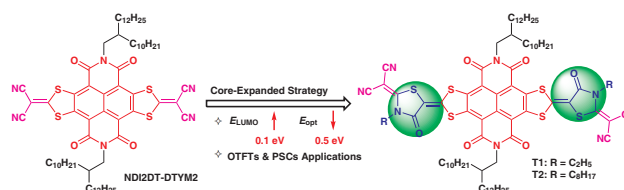# Rhodanine-Bridged Core-Expanded Naphthalene Diimide Derivatives for n-Type Semiconductors

Jiangao Li[a]
Jing Li[a]
Congwu Ge*[a]
Xike Gao*[a]

[a] Key Laboratory of Synthetic and Self-Assembly Chemistry for Organic Functional Molecules, Shanghai Institute of Organic Chemistry, University of Chinese Academy of Sciences, Chinese Academy of Science, 345 Lingling Road, Shanghai 200032 (China)
gaoxk@mail.sioc.ac.cn

Abstract The core expansion of naphthalene diimides (NDIs) is an effective strategy to modulate frontier molecular orbital energy levels and improve device performances. Herein two new rhodanine-bridged and core-extended NDIs **T1** and **T2** were designed and synthesized. The rhodanine moiety could act not only as a π-spacer to enlarge the molecular conjugated system, but also as an electron-donating unit to tune the molecular energy levels. As a result, both **T1** and **T2** showed slightly lower lying LUMO energy levels ($< - 4.2$ eV) by $ca.$ 0.1 eV and narrower optical band gaps ($ca.$ 1.5 eV) by 0.5 eV compared to those of n-type organic semiconductor (OSC) NDI2DT-DTYM2.The solution-processed organic thin-film transistors based on **T1** and **T2** exhibited electron motilities in the range of 10^{-4}–10^{-3} cm^2 V^{-1} s^{-1}, and the inverted perovskite solar cells constructed using **T2** as electron transport materials provided a power conversion efficiency value of 8.82%. The results demonstrated that embedding rhodanine units in a NDI2DT-DTYM2 backbone is an effective approach to tune the energy levels and optical properties of OSCs, providing a new way to construct novel n-type OSCs with multifunctional optoelectronic applications.

Introduction

As the key active-layer components of organic optoelectronic devices, organic semiconductor (OSC) materials have attracted considerable attention owing to their various advantages such as mechanical flexibility, low cost, solution-processability, and tunable frontier molecular orbital energy levels by rational molecular design.[1–7] Suitable HOMO and LUMO energy levels are a vital prerequisite for achieving high-performance OSCs.[8] For instance, the high-

lying HOMO and low-lying LUMO energy levels should be close to the work function of the electrode, which are beneficial for hole and electron injection, respectively, and in turn to achieve high charge carrier mobility in organic thin-film transistor (OTFT) devices.[9] In addition, a good alignment of the LUMO energy levels with the conducting band minimum of the perovskite materials is also important for the dynamics of charge transfer and extraction behavior at the perovskite–electron transport material (ETM) interface, which play an important role in determining the performance parameters such as open-circuit voltage (V_{oc}), short-circuit density (J_{sc}) as well as the power conversion efficiency (PCE).[10] The construction of π-expanded conjugated semiconductors with the push–pull strategy is one of the most successful approaches to modulate the HOMO and LUMO energy levels of OSCs.[11] In this manner, more and more extended π-conjugated OSCs with high performance burgeoned during the past decades.[12,13]

1,4,5,8-Naphthalene diimides (NDIs),[12,14,15] among the most versatile and fascinating class of building blocks, have been the subject of great research interest due to their intrinsic properties such as high electron affinity, good charge carrier mobility, and remarkable thermal and oxidative stability. As a result, the past decades have witnessed extensive developments of NDIs[14,15] as organic conjugated frameworks for the synthesis of multifunctional structures in supramolecular chemistry, chemical sensors, molecular switching devices, biomedical application, and OTFT and photovoltaic devices. At present, the chemical-structure modifications of NDIs are mainly focused on the following three paths: (i) the modulation of N-substituent alkyl chains for influencing solution processability, molecular packing, film microstructure, and in turn to tune charge transport of OTFT devices[16–18]; (ii) the core modification of NDIs including σ-bond-linked substituents (including electron-withdrawing groups and electron-donating units) for modulating molecular optical/electronic properties[19–21]; (iii) the lateral core expansion of NDIs by fusing five- and six-membered rings either on one side or both sides of the NDI core to regulate the HOMO and LUMO energy levels as well as the intramolecular and/or intermolecular interactions for efficient charge transport.[22,23]

Among such heterocyclic (carbazole, imidzaole, thiophene rings, etc.) fused NDIs,[16–23] NDI-DTYM2 derivatives bearing two (1,3-dithiol-2-ylidene)malononitrile (DTYM) are the most representative building blocks, which exhibit excellent electron mobilities and ambient stability in OTFT devices.[5a] Therefore, the core expansion of NDIs by sulfur-containing heterocycles and end capped with an electron-withdrawing group is a successful strategy to obtain high-performance OSCs. On the other hand, sulfur-heterocycle-fused NDI materials, which effectively function as nonfullerene ETMs in "regular" or "inverted" perovskite solar cells (PSCs), have far less been explored.[15a] Consequently, novel n-type OSCs based on large π-conjugated NDIs for OTFT and PSC applications are still in urgent pursuit.

To further develop core-expanded NDI chemistry, here we report two rhodanine-bridged NDI derivatives **T1** and **T2** (Scheme 1) synthesized via the core-expanded strategy. This molecular design is based on the following considerations: (i) the incorporation of π-conjugated spacer rhodanine not only extends the π-conjugation of NDIs, but also acts as a second "donor" moiety to modulate the optical/electronic properties of the molecules[24]; (ii) the selection of malononitrile as the end-capped electron-withdrawing group, which could effectively deepen the LUMO energy levels of A-π-D-A-D-π-A-type conjugated small molecules, which are crucial for achieving ambient-stable electron injection and conduction in their OTFT devices.[5a,17a]

Results and Discussion

The synthetic routes of **T1** and **T2** are shown in Scheme 1, and the synthetic details of the intermediate **A3** and **T1** and **T2** are provided in the Supporting Information (Scheme S1-S4).[25] The facile nucleophilic aromatic substitution reaction (S_NAr) of **A3** could be performed efficiently via a mild one-pot synthetic method with a yield of 51.2% for **T1** and 67.2% for **T2**, respectively.[17a] This one-pot synthesis undergoes an in-situ formation of rhodanine-bridged dithiolate sodium salts (first step) and then an S_NAr reaction (second step) in THF at room temperature, allowing an easy and low-cost access to diverse 1,3-disulfur heterocyclic-
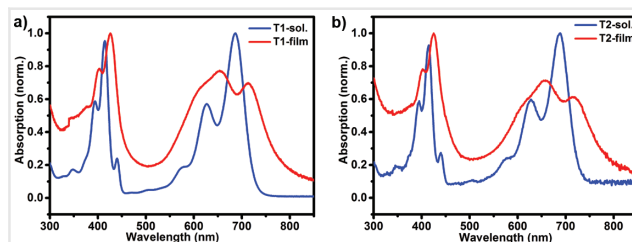

Figure 1 Normalized UV-vis-NIR absorption spectra of (**a**) **T1** and (**b**) **T2** in solution and in thin films.

fused NDI-based n-type semiconductors. A mixture of *trans/cis* target compounds (**T1** and **T2**) was obtained but the separation of the *trans*-**T1** and *cis*-**T1** (as well as the *trans*-**T2** and *cis*-**T2**) failed with column chromatography and high-performance liquid chromatography, which probably ascribed to identical molecular polarity of the *trans*- and *cis*- isomers. The chemical structures of **A3**, **T1**, and **T2** (*trans*-/*cis*- isomers) were well characterized by ^{1}H and ^{13}C NMR spectroscopy, high-resolution mass spectroscopy, FT-IR analysis as well as elemental analysis (Figure S8-S24). Both **T1** and **T2** are readily soluble in common organic solvents such as chloroform, chlorobenzene, and 1,2-dichlorobenzene (>5 mg/mL) at room temperature, allowing the solution-processable fabrication of optoelectronic devices based on them. Thermogravimetric analysis (TGA) measurements revealed that **T1** and **T2** have excellent thermal stability with decomposition temperatures (T_d, 5% weight loss) of 387 °C and 380 °C, respectively (Figure S1). Differential scanning calorimetry (DSC) characterization was also carried out under an inert atmosphere, and no apparent thermal transition signal for **T1** and **T2** was observed in the entire scanning range: 25–350 °C (Figure S2). The results indicated that **T1** and **T2** exhibit good thermal stability and their thin films can be treated over a broad range of annealing temperatures.[26]

The ultraviolet–visible–near infrared (UV-vis-NIR) absorption spectra of **T1** and **T2** in chlorobenzene solution and in thin films were measured to investigate their optical properties (Figure 1); the corresponding data are summarized in Table 1. The absorption spectra of NDI2DT-DTYM2 in solution and in thin film were also recorded for
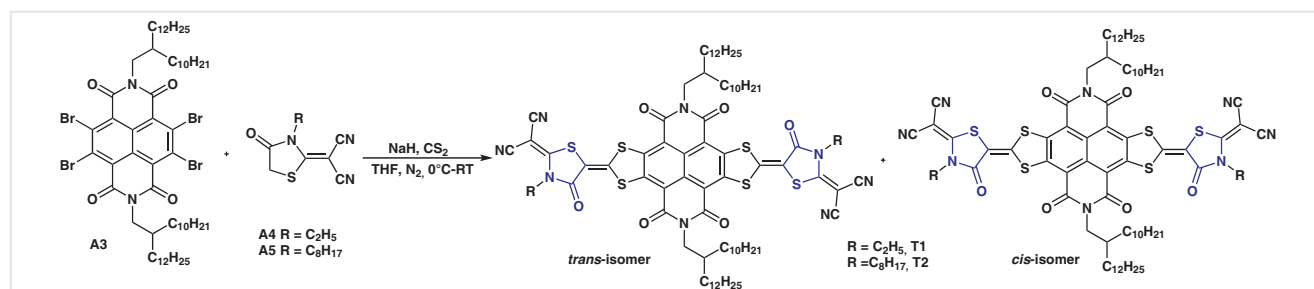
Scheme 1 Synthetic route of **T1** and **T2**.

167

Organic Materials   J. Li et al.   THIEME OPEN ACCESS   **Original Article**

Table 1 Thermal, optical, and electrochemical data for T1 and T2

Compound	T_d (°C)	λ_{max} sol. (nm)	λ_{max}^{0-0} sol. (nm)	λ_{max}^{0-1} sol. (nm)	λ_{max}^{0-0} film (nm)	λ_{max}^{0-1} film (nm)	E_g^{opt} (eV)[a]	E_{LUMO} (eV)[b]	E_{HOMO} (eV)[c]
T1	387	414	686	627	713	652	1.51	−4.20	−5.71
T2	380	414	688	627	713	654	1.49	−4.20	−5.69

[a]Estimated from the onset absorption of thin films.
[b]Calculated from the first onset reductive potential. $E_{LUMO} = -4.44 - E_{red1}^{onset}$.
[c]$E_{HOMO} = E_{LUMO} - E_g^{opt}$.

comparison (Figure S3). As shown in Figure 1, both in dilute chlorobenzene solution and in thin films, **T1** and **T2** display a typical dual-band absorption feature covering 300–800 nm. The sharp one at the high-energy region (350–500 nm) is attributed to π-–π^* transitions of the conjugated backbone, and the strong and wide absorption (550–800 nm) can be ascribed to the strong intramolecular charge transfer transition between the donor and acceptor units.[17,27] The chemically similar structures of **T1** and **T2** bearing different amide alkyl chains in rhodanine units show nearly identical absorption spectra both in solution and in thin films with nearly identical peak values of their maximum and onset absorptions (Table 1), suggesting that their optical properties are insensitive to the structure of the N-alkyl chain in the rhodanine moiety as expected.[12a] The maximum of the 0–0 vibrational peak of thin films shows a large red shift of about 25 nm compared to those of **T1** and **T2** in solution. Moreover, the absorption intensities of the 0–1 and 0–0 vibrational peaks from solution to thin film changed greatly, indicating the highly changed conformation of **T1** and **T2**, and probably the stronger intermolecular π–π stacking in the solid state originated from the J-type aggregate pattern.[28] It is worth noting that the absorptions of **T1** and **T2** in thin films extend to the NIR region with the absorption onset at 821 and 832 nm, respectively, and the corresponding E_g^{opt} values of 1.51 and 1.49 eV, respectively. In comparison with NDI2DT-DTYM2 (E_g^{opt} = 2.0 eV), the dramatic down-shift band gaps of **T2** and **T2** possibly ascribe to the larger extension of the π-conjugated system of **T1** and **T2** with the implanted

rhodanine unit as a spacer. Thus, implanting rhodanine units into OSC backbones is a potent strategy to impact on their intramolecular and intermolecular interactions and efficiently tunes the optical properties of OSC materials.[24]

To investigate the electrochemical properties of **T1** and **T2**, cyclic voltammetry (CV) measurements were performed (Figure 2 and Table 1). Compounds **T1** and **T2** exhibit a nearly identical irreversible reduction process in CHCl$_3$, in which the first onset reductive potential (E_{red1}^{onset}) is at approximately –0.24 V. The LUMO energy levels, estimated by CV [$E_{LUMO} = - (E_{red1}^{onset} + 4.44)$ eV],[29] are both at −4.20 eV. Compared to NDI2DT-DTYM2, the LUMO energy levels of **T1** and **T2** are shifted upward by ca. 0.1 eV, which is likely due to the rhodanine unit that not only as a π-conjugated spacer regulates its optical properties (Figure 1), but also as a relatively strong electron-donating moiety effectively tunes its electronic structure (Figure 2). The relative low-lying LUMO energy levels of **T1** and **T2** enable them to be potential n-type OSCs.

To evaluate the semiconducting properties of **T1** and **T2**, OTFT devices were fabricated by spin-coating the solutions of **T1** and **T2** onto octadecyl trichlorosilane (OTS)-modified Si/SiO$_2$ substrates. Au source/drain electrodes were deposited on the active layer to afford OTFTs with a bottom-gate top-contact device configuration. The OTFT devices were tested in a glovebox with a nitrogen atmosphere, and the OTFT characteristics of the devices, thermal annealed at different temperatures, are collected in Table 2. Additionally, the histograms of performance distributions of **T1**- and **T2**-based OTFT devices are
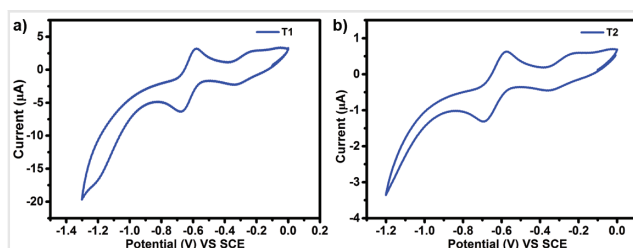

Figure 2 CV plots of **T1** and **T2** in chloroform solution. The CV plots were measured by using 0.1 M n-Bu$_4$NPF$_6$ as the supporting electrolyte, SCE as the reference electrode, Pt disk as the working electrode, and Pt wire as the counter electrode at a scan rate of 100 mV/s.

Table 2 Characteristics of OTFT devices based on thin films of T1 and T2

Compound	T_a (°C)	μ_e Max (Avg) (cm^2 V^{-1} s^{-1})[a]	V_T (V)[a]	I_{on}/I_{off}[a]
T1	As-spun	2.82×10^{-3} (1.44×10^{-3})	−3.11–8.73	10^3–10^5
	80	4.11×10^{-3} (1.76×10^{-3})	7.18–14.67	10^3–10^5
	120	2.27×10^{-3} (1.52×10^{-3})	14.70–18.33	10^3–10^5
T2	As-spun	0.27×10^{-3} (0.19×10^{-3})	2.22–13.37	10^2–10^4
	80	0.39×10^{-3} (0.20×10^{-3})	1.57–6.43	10^2–10^4
	120	0.15×10^{-3} (0.12×10^{-3})	4.13–6.10	10^2–10^4

[a]The performance data were obtained based on at least 10 different devices.
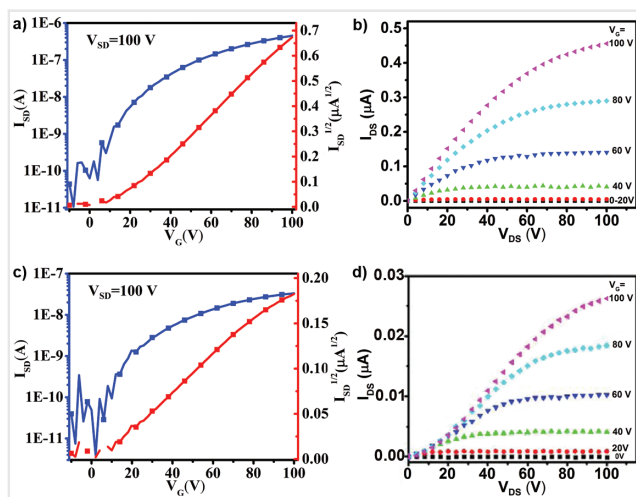
Figure 3 Transfer and output characteristics of OTFT devices based on **T1** (a, b) and **T2** (c, d).

Figure 4 AFM images of as-spun and annealed thin films of **T1** (a–c) and **T2** (d–f).

presented in Figure S5. As shown in Figure 3, all the devices exhibited n-type semiconductor characteristics, which correlate well with the aforementioned CV results (Figure 2). The as-spun OTFT devices based on compounds **T1** and **T2** showed electron mobilities (μ_e) in the range of 10^{-3}–10^{-4} cm^2 V^{-1} s^{-1}, and current on/off ratios ($I_{on/off}$) in the range of 10^2–10^5. When subjected to thermal annealing at 80 °C, the μ_e values of OTFTs with thin films of **T1** and **T2** were improved (Table 2). For instance, the as-spun OTFT devices based on **T1** showed an average μ_e value of 1.44×10^{-3} cm^2 V^{-1} s^{-1}, and a current on/off ratio ($I_{on/off}$) of 10^3–10^5. For OTFT devices based on **T1** and annealed at 80 °C, the average μ_e was enhanced to 1.76×10^{-3} cm^2 V^{-1} s^{-1} and its maximum μ_e up to 4.11×10^{-3} cm^2 V^{-1} s^{-1}. A slight decrease in mobility of the **T1**-based OTFT devices was observed after annealing at 120 °C. The performance of OTFTs based on **T2** exhibit analogous response to thermal-annealing treatment. After annealing at 80 °C, the optimal μ_e of 3.9×10^{-4} cm^2 V^{-1} s^{-1} was obtained for the **T2**-based OTFT devices (Table 2). It should be mentioned that the **T1**-based devices show about 1 order of magnitude higher μ_e values than those of **T2**-based ones. The drastically different performance of OTFT devices is probably the result of different film microstructures influenced by the alkyl chain in the rhodanine moiety, which will be discussed below.[30]

To investigate the different device performances of **T1** and **T2**, the surface morphologies, crystallinity, and microstructures of the thin films of **T1** and **T2** were analyzed by using atomic force microscopy (AFM) and X-ray diffraction (XRD), which play an important role in affecting the electronic properties.[4,30] Figure 4 shows the AFM images
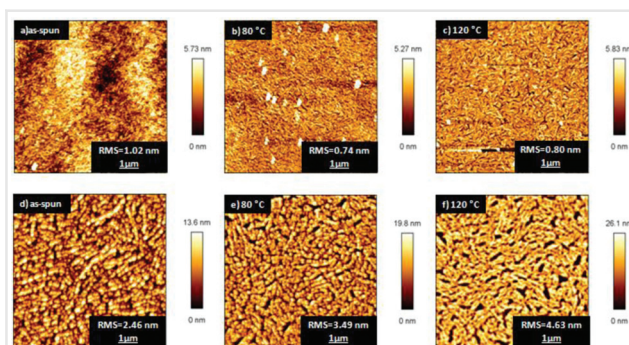
of the as-spun and annealed thin films of **T1** (Figure 4a–c) and **T2** (Figure 4d–f) deposited on an OTS-modified Si/SiO$_2$ substrate, respectively. **T1** exhibited a much smoother and uniform film morphology with a very small root-mean-square (RMS) surface roughness of about 1 nm compared to that of **T2** (RMS values of 2.46–4.63 nm), which is beneficial for charge accumulation and transport in the conducting channel and might account for the better electron-transporting property of **T1**. Moreover, the thin films of **T1** display no appreciable change (RMS values of 1.02–0.80 nm) upon annealing at 80 °C and 120 °C, respectively. In contrast, the surface morphologies of **T2** were changed drastically with large and discontinuous domains (RMS value of up to 4.63 nm) after thermal annealing as shown in Figure 4f. Such high surface roughness and large domain boundaries of **T2**-based thin films are deleterious for electron transport.[25b,30] The XRD images of **T1**- and **T2**-based thin films showed no apparent diffraction peaks even after high-temperature thermal annealing (Figure S4), suggesting their randomly arranged packing on the substrate.[31]

Finally, the potential of rhodanine-embedded NDI2DT-DTYM2 as non-fullerene ETM in PSC devices was investigated. We first evaluated the electron motilities of **T2** and NDI2DT-DTYM2 using the space-charge-limited current (SCLC) method with a device configuration of ITO/ZnO/**T2** (or NDI2DT-DTYM2)/Al. **T2** showed a SCLC electron mobility of 2.72×10^{-4} cm^2 V^{-1} s^{-1}, which is about 1 order of magnitude higher than that of NDI2DT-DTYM2 (2.64×10^{-5} cm^2 V^{-1} s^{-1}, Figure S6). For **T2**, in consideration of its high electron charge transport in the vertical direction, better solubility in common organic solvents, and the LUMO energy level's well alignment with the conducting band minimum of MAPbI$_3$,[15a,10] PSC devices using **T2** as ETMs with the inverted structure of ITO/PTAA/MAPbI$_3$/**T2**(or NDI2DT-DTYM2)/BCP/Ag were fabricated. Figures 5 and S7 depict the representative current density–
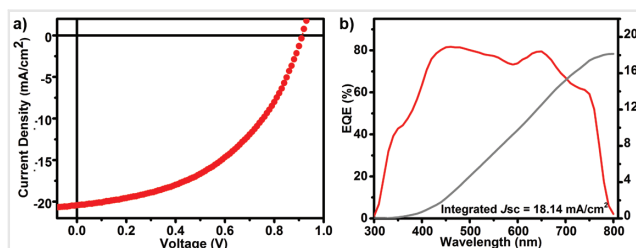
Figure 5 (a) J–V curve and (b) EQE spectra of the optimal PSC device with **T2** as ETMs.

voltage (J–V) curve and external quantum efficiency (EQE) spectra of **T2**- or NDI2DT-DYTM2-based PSCs, respectively, and the corresponding performance parameters of PSCs are collected in Table S1. The PSC devices with **T2** as the ETMs produced a J_{sc}, V_{oc}, and PCE value of 20.43 mA cm^{-2}, 0.91 V, and 8.82%, respectively, which are slight higher than those of NDI2DT-DTYM2-based PSCs (Table S1). The inverted PSC devices using **T2** as ETMs showed an EQE response from 300 to 800 nm with the maximum value of 81.7%, and the integrated J_{sc} of 18.14 mA cm^{-2} was obtained from the EQE curve.

Conclusions

In summary, **T1** and **T2** have been designed and efficiently synthesized via an effective strategy that incorporated a rhodanine unit into the core-expanded NDI2DT-DTYM2 backbone. Compared to NDI2DT-DTYM2, both **T1** and **T2** showed higher LUMO energy levels (< -4.20 eV) and lower optical band gaps (ca. 1.5 eV), demonstrating that rhodanine units play a significant role in tuning the optical and electronic properties of **T1** and **T2**. The OTFT devices based on **T1** and **T2** exhibit n-type semiconducting properties with μ_e of about10^{-3} cm^2 V^{-1} s^{-1}, and the inverted PSC devices using **T2** as ETMs displayed a decent J_{sc}, V_{oc}, and PCE value of 20.43 mA cm^{-2}, 0.91 V, and 8.82%, respectively. The above results indicate that the core-extended strategy by embedding a rhodanine unit into the backbone of OSCs is applicable and promising for constructing new families of high performance n-type semiconductors with multifunctional applications.

Experimental Section

Materials and General Method

1,4,5,8-NDA, DBH, PBr$_3$, H$_2$SO$_4$, malononitrile, octyl isothiocyanate, and A4 were purchased from Shanghai Aldrich and used as received. THF was dried using sodium and freshly distilled prior to use. CH$_3$NH$_2$ was obtained from

Energy Chemical, China. HI, 55–58 wt% in water, was purchased from Aladdin, China. Bathocuproine (BCP) was purchased from TCI, Japan. Dimethylsulphoxide (DMSO) and N,N-dimethylformamide (DMF) were obtained from J & K, China. Indium tin oxide-coated(ITO) glasses were purchased from Kaivo, China. Aluminum (Al) was purchased from Cuibolin, China. Silver (Ag) was purchased from CNM, China. ^{1}H NMR (400 MHz) and ^{13}C NMR (100 MHz) spectra were measured in deuterated chloroform (CDCl$_3$) on JEOL RESO-NANCE ECZ 400S instruments. Mass spectra (MALDI-TOF) were recorded on a Voyager-DE STR mass spectrometer. Elemental analyses were carried out on an Elementar Vario EL III elemental analyzer. TGA measurements were performed on a TA Q500 instrument under a dry nitrogen flow at a heating rate of 10 °C/min, heating from room temperature to 500 °C. DSC analyses were carried out on a Perkin Elmer Pyris 1 instrument under a dry N$_2$ flow at a heating rate of 10 °C/min, heating from room temperature to 350 °C. The electrochemical measurements for **T1**, **T2**, and NDI2DT-DTYM2 were performed on a CHI610D electrochemical work station in a conventional three-electrode cell using a platinum working electrode, a platinum-wire auxiliary electrode, and a saturated calomel electrode (SCE) reference electrode in a solution of [Bu$_4$N][PF$_6$] (0.1 M) in CHCl$_3$ at a scan rate of 100 mV/s. The experiments were calibrated with the standard ferrocene/ferrocenium (F_c) redox system and assumption that the energy level of F_c is 4.8 eV below vacuum. Optical absorption was measured on a JASCO V-570 UV-vis-NIR spectrophotometer. XRD measurements were carried out in the reflection mode with Cu Kα radiation using a Panalytical X'Pert Pro XRD system. AFM was recorded on a JPK atomic force microscope by an AC mode with a silicon tip. The current density–voltage (J–V) characteristics of the devices were measured with a Keithley 2420 measurement source unit maintained at room temperature in a N$_2$-filled glovebox. Photocurrent was acquired upon irradiation using an AAA solar simulator (Oriel 94043A, 450 W, USA) with an AM 1.5 G filter. Light intensity was simulated to be 100 mW cm^{-2} using a NREL-certified standard silicon cell (Oriel reference cell 91150, USA). EQE was measured with a 75 W xenon lamp that was equipped with an Oriel monochromator (74125), an optical chopper, a lock-in amplifier, and an NREL-calibrated crystalline silicon cell.

Device Fabrication and Characterization

OTFT device fabrication and characterization: The OTFT devices based on **T1** and **T2** were fabricated by a spin-coating method with a bottom-gate top-contact (BG/TC) configuration with a channel length of 31 μm and a width of 273 μm. The Si/SiO$_2$ substrates were cleaned via a standard procedure. The Si/SiO$_2$ substrates were modified with octadecyltrichlorosilane (OTS) on the surface via a vapor

deposition method for about 4 hours. Then, the substrates were rinsed with chloroform, *n*-hexane, acetone, and isopropyl alcohol subsequently by ultrasonic cleaning for 5 min, respectively. Then, the Si/SiO$_2$ substrate was dried with N$_2$ quickly. The active layers were fabricated on the OTS-treated substrate by spin-coating with the small-molecule solutions in chlorobenzene for T1 (5 mg mL^{-1}) and in chloroform for T2 (10 mg mL^{-1}), respectively. Finally, Au was used as a source and drain electrode, and was deposited on the top of the semiconducting layer through a shadow mask under high vacuum. The device performances were measured with a Keithley 4200 semiconductor parameter analyzer. The mobilities were calculated from the equation: $I_{DS} = (\mu W C_i/2L)(V_{GS} - V_T)^2$, where I_{DS} is the source-drain current, μ is the carrier mobility, C_i is the capacitance per unit area of the dielectric layer (10 nF/cm^2), V_{GS} and V_T are the gate voltage and threshold voltage, respectively.

PSCs device fabrication and characterization: ITO glass was cleaned using detergent, deionized water, acetone, and isopropanol ultrasonic baths step by step for 20 min before drying in a N2 flow, respectively. Then the ITO substrate was cleaned by ultraviolet ozone (UVO) for 20 min. A thin layer of PTAA was spin-coated onto the cleaned ITO at 4000 rpm for 60 s, and annealed at 140 °C for 15 min. Finally the ITO-coated substrates were transferred into a N$_2$-filled glovebox for active layer deposition and further device fabrication. The active layer was deposited via a two-step procedure: first step: a precursor mixture solution with PbI$_2$: MAI = 1.3: 0.3 M in a mixture of DMF and DMSO (9:1, v:v); second step: a solution with MAI 55 mg/mL in isopropanol (IPA) was spin-coated onto the PTAA-coated-ITO (ITO-PTAA) substrate at 1000 rpm for 10 s and 4000 rpm for 50 s, respectively, and then annealed at 90 °C for 30 min. After cooling of the PSC active layer to room temperature, the **T2** (10 mg/mL) and BCP (0.5 mg/mL in IPA) solutions were used to deposit subsequently at 1000 rpm for 30 s and 4000 rpm for 40 s at room temperature, respectively. Finally, 100 nm of Ag film was thermal evaporated as counter electrodes using a shadow mask to finish the device fabrication process. The accurate active cell area of the device by the overlap of the electrodes was about 0.04 cm^2. The *J–V* characteristics of the PSCs were measured with a Keithley 2420 measurement source unit maintained at room temperature in the N$_2$-filled glovebox. Photocurrent was acquired upon irradiation using an AAA solar simulator (Oriel 94043A, 450 W, USA) with an AM 1.5 G filter. Light intensity was simulated to be 100 mW/cm^2 using an NREL-certified standard silicon cell (Oriel reference cell 91150, USA). EQE was measured with a 75 W xenon lamp that was equipped with an Oriel monochromator (74125), an optical chopper, a lock-in amplifier, and an NREL-calibrated crystalline silicon cell.

Synthetic Part

*Compound **T1***: Under a nitrogen atmosphere, a solution of CS$_2$ in THF was added slowly to NaH (120 mg, w = 60%, 3 mmol) at 0 °C, and then stirred at room temperature for 4 hours. The mixture was added to **A3** solution (125.5 mg, 0.1 mmol) and stirred at room temperature for another 1 hour. After the reaction was completed, some water was added to the mixture and extracted with chloroform. The combined organic layer was dried using Na$_2$SO$_4$ and the filtrate was concentrated under reduced pressure. Chromatography of the residue on a silica gel column with dichloromethane/petroleum ether (1/1) as an eluent afforded **T1** as a bluish green solid (120 mg, yield: 51.2%). Mp > 300 °C. ^{1}H NMR (400 MHz, CDCl$_3$) δ 4.35 (dd, J = 13.2, 6.2 Hz, 4H), 4.27 (d, J = 7.2 Hz, 4H), 2.07 (d, J = 4.1 Hz, 2H), 1.48 (t, J = 5.9 Hz, 6H), 1.39–1.15 (m, 80H), 0.89–0.81 (m, 12H). ^{13}C NMR (100 MHz, CDCl$_3$) δ = 165.98, 165.16, 164.94, 150.72, 150.30, 145.85, 128.37, 119.60, 44.48, 39.71, 34.87, 33.11, 32.67, 29.57, 25.59, 16.98. FT-IR (KBr): 2922.5, 2851.6, 2216.4, 1694.6, 1636.9, 1526.1, 1457.1, 1388.5, 1375.1, 1338.1, 1295.1, 1212.7, 1088.8, 1070.3, 882.5, 837.1, 784.0, 739.0, 726.8, 693.3, 630.7, 547.0, 503.7, 461.5 cm^{-1}. MS (MALDI-TOF) *m/z*: 1469.6716 (M + H)$^+$; HR-MS (MALDI-TOF) (M + H)$^+$ calcd for C$_{80}$H$_{108}$N$_8$O$_6$S$_6$: 1469.6716; found: 1469.6788. Anal. calcd. for C$_{80}$H$_{108}$N$_8$O$_6$S$_6$ (%): C, 65.36; H, 7.40; N, 7.62; found: C, 65.53; H, 7.50; N, 7.58.

*Compound **T2***: A similar synthesis and purification method to **T1** was implemented for the preparation of **T2** (220 mg, yield 67.2%), by using **A5** instead of **A4**. Mp > 300 °C. ^{1}H NMR (400 MHz, CDCl$_3$) δ 4.26 (dd, J = 13.3, 6.6 Hz, 8H), 2.06 (ddd, J = 18.3, 13.1, 5.6 Hz, 2H), 1.46–1.17 (m, 104H), 0.92–0.82 (m, 18H). ^{13}C NMR (100 MHz, CDCl$_3$) δ = 163.02, 162.06, 161.77, 117.02, 111.89, 46.20, 36.61, 31.93, 31.75, 31.61, 30.19, 29.71, 29.38, 29.11, 26.29, 22.66, 14.11. FT-IR (KBr): 2921.1, 2851.6, 2214.8, 1733.1, 1716.6, 1694.4, 1652.6, 1636.2, 1526.5, 1506.8, 1456.4, 1385.0, 1338.3, 1295.3, 1209.6, 1167.4, 829.2, 784.0, 739.4, 632.9, 580.8, 418.8 cm^{-1}. LRMS: (MALDI-TOF) (M + H)$^+$ calcd for C$_{92}$H$_{132}$N$_8$O$_6$S$_6$: 1638.8628; found: 1638.3. Anal. calcd. for C$_{92}$H$_{132}$N$_8$O$_6$S$_6$ (%): C, 67.44; H, 8.12; N, 6.84; found: C, 67.46; H, 7.94; N, 6.72.

Funding Information

Supporting Information

Supporting information for this article is available online at http://doi.org/10.1055/s-0040-1710550.

References

(1) (a) Dong, H.; Fu, X.; Liu, J.; Wang, Z.; Hu, W. *Adv. Mater.* **2013**, *25*, 6158. (b) Dennler, G.; Scharber, M.; Brabec, C. *Adv. Mater.* **2009**, *21*, 1323. (c) Yang, Z.; Mao, Z.; Xie, Z.; Zhang, Y.; Liu, S.; Zhao, J.; Xu, J.; Chi, Z. *Chem. Soc. Rev.* **2017**, *46*, 915. (d) Han, S.; Peng, H.; Sun, Q.; Venkatesh, S.; Chung, K.; Lau, S.; Zhou, Y.; Roy, V. *Adv. Mater.* **2017**, *29*, 1700375. (e) Zaumseil, J.; Sirringhaus, H. *Chem. Rev.* **2007**, *107*, 1296. (f) Murphy, A. R.; Fréchet, J. M. *Chem. Rev.* **2007**, *107*, 1066. (g) Usta, H.; Facchetti, A.; Marks, T. J. *Acc. Chem. Res.* **2011**, *44*, 501. (h) Klauk, H. *Chem. Soc. Rev.* **2010**, *39*, 2643. (i) Torrent, M.; Rovira, C. *Chem. Soc. Rev.* **2008**, *37*, 827.

(2) (a) Wang, C.; Dong, H.; Hu, W.; Liu, Y.; Zhu, D. *Chem. Rev.* **2012**, *112*, 2208. (b) Mandal, S.; Noh, Y. Y. *Semicond. Sci. Technol.* **2015**, *30*, 064003. (c) Tong, S.; Sun, J.; Yang, J. *ACS Appl. Mater. Interfaces* **2018**, *10*, 25902.

(3) (a) Yu, Y.; Ma, Q.; Ling, H.; Li, W.; Ju, R.; Bian, L.; Shi, N.; Qian, Y.; Yi, M.; Xie, L.; Huang, W. *Adv. Funct. Mater.* **2019**, *29*, 1904602. (b) Sui, Y.; Deng, Y. F.; Du, T.; Shi, Y.; Geng, Y. *Mater. Chem. Front.* **2019**, *3*, 1932. (c) Ren, Y.; Yang, X.; Zhou, L.; Mao, J.; Han, S.; Zhou, Y. *Adv. Funct. Mater.* **2019**, *29*, 1902105.

(4) (a) Di, C. A.; Zhang, F.; Zhu, D. *Adv. Mater.* **2013**, *25*, 313. (b) Zhang, F.; Di, C. A.; Berdunov, N.; Hu, Y.; Hu, Y. B.; Gao, X.; Meng, Q.; Sirringhaus, H.; Zhu, D. *Adv. Mater.* **2013**, *25*, 1401. (c) Zhao, Y.; Di, C. A.; Gao, X.; Hu, Y.; Guo, Y.; Zhang, L.; Liu, Y.; Wang, J.; Hu, W.; Zhu, D. *Adv. Mater.* **2011**, *23*, 2448.

(5) (a) Gao, X.; Di, C. A.; Hu, Y.; Yang, X.; Fan, H.; Zhang, F.; Liu, Y.; Li, H.; Zhu, D. *J. Am. Chem. Soc.* **2010**, *132*, 3697. (b) Minemawari, H.; Yamada, T.; Matsui, H.; Tsutsumi, J.; Haas, S.; Chiba, R.; Kumai, R.; Hasegawa, T. *Nature* **2011**, *475*, 364. (c) Zhang, F.; Di, C. A.; Berdunov, N.; Hu, Y.; Gao, X.; Meng, Q.; Sirringhaus, H.; Zhu, D. *Adv. Mater.* **2013**, *25*, 1401.

(6) (a) Sokolov, A. N.; Tee, B. C.; Bettinger, C. J.; Tok, J. B.; Bao, Z. *Acc. Chem. Res.* **2012**, *45*, 361. (b) Nakayama, K.; Hirose, Y.; Soeda, J.; Yoshizumi, M.; Uemura, T.; Uno, M.; Li, W.; Kang, M.; Yamagishi, M.; Okada, Y.; Miyazaki, E.; Nakazawa, Y.; Nakao, A.; Takimiya, K.; Takeya, J. *Adv. Mater.* **2011**, *23*, 1626.

(7) (a) Someya, T.; Dodabalapur, A.; Huang, J.; See, K. C.; Katz, H. E. *Adv. Mater.* **2010**, *22*, 3799. (b) Li, H.; Shi, W.; Song, J.; Jang, H.; Dailey, J.; Yu, J.; Katz, H. *Chem. Rev.* **2019**, *119*, 3.

(8) (a) Marrocchi, A.; Facchetti, A.; Lanari, D.; Petruccia, C.; Vaccaro, L. *Energy Environ. Sci.* **2016**, *9*, 763. (b) Bohra, H.; Wang, M. *J. Mater. Chem. A* **2017**, *5*, 11550–1. (c) Gu, P.; Wang, N.; Wang, C.; Zhou, Y.; Long, G.; Tian, M.; Chen, W.; Sun, X.; Kanatzidis, M.; Zhang, Q. *J. Mater. Chem. A* **2017**, *5*, 7339. (d) Wang, N.; Zhao, K.; Ding, T.; Liu, W.; Ahmed, A.; Wang, Z.; Tian, M.; Sun, X.; Zhang, Q. *Adv. Energy Mater.* **2017**, *7*, 1700522.

(9) (a) Pandey, L.; Risko, C.; Norton, J.; Bredas, J. *Macromolecules* **2012**, *45*, 6405. (b) Usta, H.; Facchetti, A.; Marks, T. J. *J. Am. Chem. Soc.* **2008**, *130*, 8580.

(10) (a) Tian, J.; Xue, Q.; Tang, X.; Chen, Y.; Li, N.; Hu, Z.; Yip, H. L. *Adv. Mater.* **2019**, *31*, 1901152. (b) Ye, Q.; Zhao, Y.; Mu, S.; Ma, F.; Gao, F.; Chu, Z.; Yin, Z.; Gao, P.; Zhang, X.; You, J. *Adv. Mater.* **2019**, *31*, 1905143. (c) Said, A.; Xie, J.; Zhang, Q. *Small* **2019**, *15*, 1900854.

(11) (a) Cheng, Y. J.; Yang, S. H.; Hsu, C. S. *Chem. Rev.* **2009**, *109*, 5868. (b) Lu, D.; Yang, X.; Leng, B.; Yang, X.; Ge, C.; Jia, X.; Gao, X. *Chin. Chem. Lett.* **2016**, *27*, 1022.

(12) (a) Hu, Y.; Gao, X.; Di, C.; Yang, X.; Zhang, F.; Liu, Y.; Li, H.; Zhu, D. *Chem. Mater.* **2011**, *23*, 1204. (b) Zhao, Y.; Di, C. A.; Gao, X.; Hu, Y.; Guo, Y.; Zhang, L.; Liu, Y.; Wang, J.; Hu, W.; Zhu, D. *Adv. Mater.* **2011**, *23*, 2448. (c) Wu, W.; Li, J.; Zhao, Z.; Yang, X.; Gao, X. *Org. Chem. Front.* **2017**, *4*, 823.

(13) (a) Suraru, S. L.; Zschieschang, U.; Klauk, H.; Würthner, F. *Chem. Commun.* **2011**, *47*, 11504. (b) Suraru, S. L.; Burschka, C.; Würthner, F. *J. Org. Chem.* **2014**, *79*, 128. (c) Gao, X.; Hu, Y. *J. Mater. Chem. C* **2014**, *2*, 3099–3117.

(14) (a) Kobaisi, M. A.; Bhosale, S. V.; Latham, K.; Raynor, A. M.; Bhosale, S. V. *Chem. Rev.* **2016**, *116*, 11685. (b) Guo, X.; Facchetti, A.; Marks, T. J. *Chem. Rev.* **2014**, *114*, 8943.

(15) (a) Ge, C., W W; Hu, L.; Hu, Y.; Zhou, Y.; Li, W.; Gao, X. *Org. Electron.* **2018**, *61*, 113. (b) Nakamura, T.; Shioya, N.; Shimoaka, T.; Nishikubo, R.; Hasegawa, T.; Saeki, A.; Murata, Y.; Murdey, R.; Wakamiya, A. *Chem. Mater.* **2019**, *31*, 1729.

(16) (a) Katz, H.; Johnson, J.; Lovinger, A.; Li, W. *J. Am. Chem. Soc.* **2000**, *122*, 7787. (b) Shukla, D.; Nelson, S.; Freeman, D.; Rajeswaran, M.; Ahearn, W.; Meyer, D.; Carey, J. *Chem. Mater.* **2008**, *20*, 7486. (c) Luo, H.; Liu, Z.; Cai, Z.; Wu, L.; Zhang, G.; Liu, C.; Zhang, D. *Chin. J. Chem.* **2012**, *30*, 1453.

(17) (a) Hu, Y.; Qin, Y.; Gao, X.; Zhang, F.; Di, C.; Zhao, Z.; Li, H.; Zhu, D. *Org. Lett.* **2012**, *14*, 292. (b) Katz, H. E.; Lovinger, A. J.; Johnson, J.; Kloc, C.; Siegrist, T.; Li, W.; Lin, Y.; Dodabalapur, A. *Nature* **2000**, *404*, 478.

(18) (a) Suraru, S.; Würthner, F. *Angew. Chem. Int. Ed.* **2014**, *53*, 7428. (b) Fan, W.; Liu, C.; Li, Y.; Wang, Z. *Chem. Commun.* **2016**, *53*, 188.

(19) (a) Kim, R.; Amegadze, P.; Kang, I.; Yun, H.; Noh, Y.; Kwon, S.; Kim, Y. *Adv. Funct. Mater.* **2013**, *23*, 5719. (b) Liu, Z.; Zhang, G.; Cai, Z.; Chen, X.; Luo, H.; Li, Y.; Wang, J.; Zhang, D. *Adv. Mater.* **2014**, *26*, 6965. (c) Gsänger, M.; Bialas, D.; Huang, L.; Stolte, M.; Würthner, F. *Adv. Mater.* **2016**, *28*, 3615.

(20) (a) Chen, Z.; Zheng, Y.; Yan, H.; Facchetti, A. *J. Am. Chem. Soc.* **2009**, *131*, 8. (b) Yan, H.; Chen, Z.; Zheng, Y.; Newman, C.; Quinn, J.; Dotz, F.; Kastler, M.; Facchetti, A. *Nature* **2009**, *457*, 679. (c) Tachapermpon, Y.; Maniam, S.; Wanichacheva, N.; Langford, S. *Asian J. Org. Chem.* **2017**, *6*, 47.

(21) (a) Jones, B.; Facchetti, A.; Marks, T.; Wasielewski, M. *Chem. Mater.* **2007**, *19*, 2703. (b) Nakano, M.; Osaka, I.; Hashizume, D.; Takimiya, K. *Chem. Mater.* **2015**, *27*, 6418. (c) Sakai, N.; Mareda, J.; Vauthey, E.; Matile, S. *Chem. Commun.* **2010**, *46*, 4225.

(22) (a) Fukutomi, Y.; Nakano, M.; Hu, J. Y.; Osaka, I.; Takimiya, K. *J. Am. Chem. Soc.* **2013**, *135*, 11445. (b) Fan, W.; Winands, T.; Doltsinis, N. L.; Li, Y.; Wang, Z. *Angew. Chem. Int. Ed.* **2017**, *56*, 15373. (c) Cui, X.; Xiao, C.; Winands, T.; Koch, T.; Li, Y.; Zhang, L.; Doltsinis, N. L.; Wang, Z. *J. Am. Chem. Soc.* **2018**, *140*, 12175.

(23) (a) Tan, L.; Guo, Y.; Zhang, G.; Yang, Y.; Zhang, D.; Yu, G.; Xu, W.; Liu, Y. *J. Mater. Chem.* **2011**, *21*, 18042. (b) Suraru, S. L.; Würthner, F. *J. Org. Chem.* **2013**, *78*, 5227. (c) Insuasty, A.; Maniam, S.; Langford, S. J. *Chemistry* **2019**, *25*, 7058. (d) Li, C.; Xiao, C.; Li, Y.; Wang, Z. *Org. Lett.* **2013**, *15*, 682.

(24) Liu, H.; Li, Z.; Zhao, D. *Sci. China Mater.* **2019**, *62*, 1574.

(25) (a) Sasikumar, M.; Suseela, Y. V.; Govindaraju, T. *Asian J. Org. Chem.* **2013**, *2*, 779. (b) Gao, X.; Qiu, W.; Yang, X.; Liu, Y.; Wang, Y.; Zhang, H.; Qi, T.; Liu, Y.; Lu, K.; Du, C.; Shuai, Z.; Yu, G.; Zhu, D. *Org. Lett.* **2007**, *9*, 3917. (c) Zhao, Z.; Zhang, F.; Hu, Y.; Wang, Z.; Leng, B.; Gao, X.; Di, C.; Zhu, D. *ACS Macro Lett.* **2014**, *3*, 1174.

(26) Luo, H. W.; Cai, Z.; Tan, L.; Guo, Y.; Yang, G.; Liu, Z.; Zhang, G.; Zhang, D.; Xu, W.; Liu, Y. *J. Mater. Chem. C* **2013**, *1*, 2688.

(27) Wu, H.; Wang, Y.; Qiao, X.; Wang, D.; Yang, X.; Li, H. *Chem. Mater.* **2018**, *30*, 6992.

(28) (a) Spano, F. C. *Acc. Chem. Res.* **2010**, *43*, 429. (b) Montoya, M.; Janssen, R. *Adv. Funct. Mater.* **2017**, *27*, 1605779. (c) Yi, Y.; Feng, H.; Zheng, N.; Ke, X.; Kan, B.; Chang, M.; Xie, Z.; Wan, X.; Li, C.; Chen, Y. *Chem. Mater.* **2019**, *31*, 904.

(29) (a) Dou, L.; Gao, J.; Richard, E.; You, J.; Chen, C.; Cha, K.; He, Y.; Li, G.; Yang, Y. *J. Am. Chem. Soc.* **2012**, *134*, 10071. (b) Chen, X.; Guo, Y.; Tan, L.; Yang, G.; Li, Y.; Zhang, G.; Liu, Z.; Xu, W.; Zhang, D. *J. Mater. Chem. C* **2013**, *1*, 1087.

(30) (a) Di, C. A.; Liu, Y.; Yu, G.; Zhu, D. *Acc. Chem. Res.* **2009**, *42*, 1573. (b) Dong, H.; Jiang, L.; Hu, W. *Phys. Chem. Chem. Phys.* **2012**, *14*, 14165. (c) Pujari, S.; Scheres, L.; Marcelis, A.; Zuilhof, H. *Angew. Chem. Int. Ed.* **2014**, *53*, 6322. (d) Magliulo, M.; Manoli, K.; Macchia, E.; Palazzo, G.; Torsi, L. *Adv. Mater.* **2015**, *27*, 7528.

(31) (a) An, C.; Puniredd, S.; Guo, X.; Stelzig, T.; Zhao, Y.; Pisula, W.; Baumgarten, M. *Macromolecules* **2014**, *47*, 979. (b) Tsao, H. N.; Cho, D. M.; Park, I.; Hansen, M.; Mavrinskiy, A.; Yoon, D.; Graf, R.; Pisula, W.; Spiess, H.; Müllen, K. *J. Am. Chem. Soc.* **2011**, *133*, 2605.